Atmospheric Environment 44 (2010) 4116–4125

Contents lists available at ScienceDirect

Atmospheric Environment

journal homepage: www.elsevier.com/locate/atmosenv

A comparison of chemical mechanisms based on TRAMP-2006 field data

Shuang Chen [a,*], Xinrong Ren [a,1], Jingqiu Mao [a,2], Zhong Chen [a,3], William H. Brune [a], Barry Lefer [b], Bernhard Rappenglück [b], James Flynn [b], Jennifer Olson [c], James H. Crawford [c]

[a] Department of Meteorology, Pennsylvania State University, 503 Walker Building, University Park, PA 16802, USA
[b] Earth and Atmospheric Sciences Department, University of Houston, Houston, TX 77204, USA
[c] NASA Langley Research Center, Hampton, VA 23681, USA

ARTICLE INFO

Article history:
Received 15 September 2008
Received in revised form
11 May 2009
Accepted 19 May 2009

Keywords:
Hydroxyl radical
Hydroperoxy radical
Model intercomparison
Chemical mechanisms
Atmospheric chemistry

ABSTRACT

A comparison of a model using five widely known mechanisms (RACM, CB05, LaRC, SAPRC-99, SAPRC-07, and MCMv3.1) has been conducted based on the TexAQS II Radical and Aerosol Measurement Project (TRAMP-2006) field data in 2006. The concentrations of hydroxyl (OH) and hydroperoxy (HO_2) radicals were calculated by a zero-dimensional box model with each mechanism and then compared with the OH and HO_2 measurements. The OH and HO_2 calculated by the model with different mechanisms show similarities and differences with each other and with the measurements. First, measured OH and HO_2 are generally greater than modeled for all mechanisms, with the median modeled-to-measured ratios ranging from about 0.8 (CB05) to about 0.6 (SAPRC-99). These differences indicate that either measurement errors, the effects of unmeasured species or chemistry errors in the model or the mechanisms, with some errors being independent of the mechanism used. Second, the modeled and measured ratios of HO_2/OH agree when NO is about 1 ppbv, but the modeled ratio is too high when NO was less and too low when NO is more, as seen in previous studies. Third, mechanism–mechanism HO_x differences are sensitive to the environmental conditions – in more polluted conditions, the mechanism–mechanism differences are less. This result suggests that, in polluted conditions, the mechanistic details are less important than in cleaner conditions, probably because of the dominance of reactive nitrogen chemistry under polluted conditions.

1. Introduction

Atmospheric hydroxyl (OH) and hydroperoxy (HO_2) radicals (collectively HO_x) play a key role in tropospheric chemistry. In urban polluted environments, the atmospheric processes involving OH and HO_2 radicals can be very complex with the abundant anthropogenic species such as NO and NO_2 (collectively NO_x) and volatile organic compounds (VOCs) (Sadanaga et al., 2003). These processes in the atmosphere can be described mathematically by a chemical mechanism, which is essential for air quality modeling. A highly explicit chemical mechanism would be preferred for the modeling because it represents the chemistry of atmosphere as accurately as possible. However, this approach is not practical due to incomplete knowledge of organic reactions and the limited availability of measurements of many higher order VOCs and oxygenated VOCs (OVOCs). Therefore, lumping approaches have been used to develop condensed chemical mechanisms that contain a limited number of reactions and unknown processes. Examples of such condensed mechanisms are Lurmann, Carter and Coyner mechanism (LCC) of Lurmann et al. (1987), Carbon Bond IV (CB4) of Gery et al. (1989), and Regional Atmospheric Chemical Mechanism (RACM) of Stockwell et al. (1997). Therefore two questions arise: (1) are these mechanisms consistent with each other? (2) how do the mechanisms compare to measurements?

Comparisons of some chemical mechanisms have been conducted in previous studies (e.g., Derwent, 1990, 1993; Olson et al., 1997; Kuhn et al., 1998; Jimenez et al., 2003; Luecken et al., 2007). As discussed in these papers, to determine the performance of a mechanism, the model results must be compared with measurements in environmental chambers or in the real atmosphere. However, while the environmental chambers have the advantage of known and controlled VOC mixtures, they have the shortcomings of chamber artifact effects and generally higher initial concentrations of VOCs and NO_x than in the real atmosphere. Alternatively, comparing *in situ* observed HO_x radicals with model

* Corresponding author. Tel.: +1 814 863 8752; fax: +1 814 865 3663.
E-mail address: suc185@psu.edu (S. Chen).
[1] Now at Rosenstiel School of Marine and Atmospheric Science, University of Miami, Miami, FL 33149, USA.
[2] Now at School of Engineering and Applied Science, Harvard University, Cambridge, MA 02138, USA.
[3] Now at Department of Atmospheric & Planetary Science, Hampton University, Hampton, VA 23668, USA.

1352-2310/$ – see front matter © 2009 Elsevier Ltd. All rights reserved.
doi:10.1016/j.atmosenv.2009.05.027

simulations has the shortcoming of possible unmeasured important atmospheric constituents, but has the advantage of evaluating chemical mechanisms in the environment of greatest interest – the atmosphere (Stockwell et al., 1997; Dodge, 2000). Unfortunately, HO_x was not measured for any of the model comparison studies that were discussed previously. One of the reasons is that until recently, the instruments have not been adequately developed to measure the major constraining atmospheric constituents that are necessary to model HO_x, particularly a large number of hydrocarbons and photolysis frequencies (Heard and Pilling, 2003). Although several measurements of HO_x radicals have been conducted under urban environments in the past decade, the comparisons with modeling results (Table 1) have generally been limited to one mechanism in the model. In most of these studies, HO_x were underestimated, sometimes by a factor of three and even larger (Table 1). Therefore, further comparisons of modeled and observed radicals, especially considering the differences of chemical mechanisms, are necessary to interpret the discrepancies and improve the mechanisms.

2. Description of chemical mechanisms

The five mechanisms compared here have been actively in use in research and regulatory applications. The recent revisions of some mechanisms are substantial enough to conduct a new comparison among these mechanisms. General characteristics of these mechanisms are summarized in Table 2. The main features for each mechanism are briefly described below.

RACM (Stockwell et al., 1997) is a revised version of the Regional Acid Deposition Mechanism (RADM2) (Stockwell et al., 1990), which was developed from the first version of RADM (Stockwell, 1986). The main revisions have been performed for organic chemistry such as the oxidation mechanisms for isoprene, α-pinene, and D-limonene. Most of the organic species are aggregated into the model species based on their similarity in functional groups and reactivity toward OH. For instance, alkenes other than ethene are represented by three species: terminal alkenes, internal alkenes, and dienes. Some organic species such as formaldehyde and isoprene are treated explicitly.

Carbon Bond Mechanism (CB05) (Yarwood et al., 2005) is updated from the version IV, CB4. In contrast to the previous version, (1) inorganic reactions are extended to simulate remote to polluted urban conditions; (2) two extensions are available to be added to the core mechanism for modeling explicit species and reactive chlorine chemistry. Organic species are lumped according to the carbon bond approach, that is, bond type, e.g., carbon single bond and double bond. Reactions are aggregated based on the similarity of carbon bond structure so that fewer surrogate species are needed in the model. For instance, the single-bonded one-carbon-atom surrogate PAR represents alkanes and most of the alkyl groups. Some organics (e.g., organic nitrates and aromatics) are lumped with the similar manners to RACM.

NASA Langley Research Center mechanism (LaRC, October 2005 version) is updated from the mechanism used in Davis et al. (1993), which adapted the NMHC oxidation mechanism from LCC with modifications to address remote low-NO_x conditions (e.g., formation of organic peroxides), includes wet and dry removal rates recommended by Logan et al. (1981). Isoprene chemistry is based on the condensed mechanism from Carter and Atkinson (1996). The lumping technique applied in LaRC is relatively simple. Alkanes, alkenes, aldehydes and aromatics are lumped together respectively. Organic nitrates and peroxides are separated into more groups than those in RACM and CB05.

Statewide Air Pollution Research Center mechanism of Carter (2000) (SAPRC-99) represents a complete update of the SAPRC-90 mechanism of Carter (1990). The mechanism described here is focused on the base mechanism combined with the extended mechanism for lumped VOCs. The main revisions were made to update reaction rates, treat some species explicitly, and condense a few mechanisms. The organic species are lumped based on the similarity of reactivity toward OH, a similar approach to RACM. Using similar but more extensive organic peroxy operators that are used in CB05, a higher condensed mechanism of the peroxy reactions is employed to limit the number of free radical species.

SAPRC-07 (Carter, 2007) is the latest version of SAPRC, which keeps the general structure of SAPRC-99 but adds chlorine chemistry. A different method with 34 steady-state radical operators

Table 1
Previous urban ground-based studies of modeled and observed HO_x radicals.

Campaign	Mechanism	Modeled-to-Observed Ratio (daytime)		Reference
		OH	HO_2	
LAFRE, summer	LCC	1–1.5	>1	George et al., 1999
SOS, summer	ADOM[a]	0.75	0.64	Martinez et al., 2003
PMTACS-NY, summer	RACM[b]	0.64[c]	0.40[c]	Ren et al., 2003b
PUMA, summer	MCMv3.1	0.58	0.56	Emmerson et al., 2005
PUMA, winter	MCMv3.1	0.50	0.49	Emmerson et al., 2005
PMTACS-NY, winter	RACM	0.62[c]	0.10[c]	Ren et al., 2006
MCMA, spring	RACM	0.79[c]	0.57[c]	Shirley et al., 2006
TORCH, summer	MCMv3.1	1.24	1.07	Emmerson et al., 2007
IMPACT-IV, winter	RACM	0.93	0.48	Kanaya et al., 2007
IMPACT-L, summer	RACM	0.86	1.29	Kanaya et al., 2007

[a] Acid Deposition and Oxidants Model mechanism (ADOM) combined with isoprene and α-pinene mechanisms from other literatures.
[b] Supplemented by detailed isoprene oxidation mechanisms from other literatures.
[c] These ratios have been adjusted based on the data corrected by absolute calibration (Ren et al., 2008; Mao et al., 2010).

Table 2
Characteristics of the chemical mechanisms.

Mechanisms	RACM	CB05	LaRC	SAPRC-99[a]	SAPRC-07[a]	MCMv3.1
Lumped type	Molecule	Structure	Molecule	Molecule	Molecule	Near-explicit
# of reactions	**237**	**156**	**279**	**211**	**291**	**13 568**
Photolysis	23	23	35	30	34	~2600
Inorganic	35	44	31	45	55	36
Organic	179	89	185	136	202[b]	~11 000
Other	–	–	28	–	–	3
# of species	**77**	**51**	**109**	**79**	**110**	**4647**
Stable inorganic	**17**	**12**	**17**	**17**	**17**	**17**
Short-lived inorganic	**4**	**4**	**5**	**4**	**9**[c]	**4**
Stable organic	**32**	**26**	**57**	**42**	**42**	**(135)**[d]
Alkanes	5	3	4	6	6	(22)
Alkenes	4	3	2	3	3	(17)
Biogenics	3	2	1	2	2	(3)
Aromatics	3	3	3	3	4	(18)
Carbonyls	9	5	10	13[e]	13	(16)
Organic nitrates	3	3	11	5	5	217
Organic peroxides	3	2	19	2	2	800
Organic acids	2	3	2	5	5	76(3)
Other	–	2	6	3	2	56
Short-lived organic	**24**	**9**	**28**	**16**	**42**[f]	**(982**[g]**)**

[a] With extended mechanism for lumped VOCs.
[b] 72 of these are reactions of steady-state peroxy radical operators.
[c] Including four steady-state inorganic operators, such as xOH.
[d] Numbers of primary emitted VOCs are shown within parentheses.
[e] Including BALD (aromatic aldehydes).
[f] Including 29 steady-state organic operators, such as xHCHO.
[g] Number of the organic peroxy radicals.

(5 of these are inorganic operators) is used to represent 72 radical reactions. An important revision is that the mechanisms for many types of VOCs are added or improved, resulting in over 20% increase of reactivity estimates. Only lumped VOCs reactions are used here to extend the base mechanism too.

Master Chemical Mechanism (MCM) is the only near-explicit chemical mechanism compared in this study. The latest version, MCMv3.1 (available at the MCM website: http://mcm.leeds.ac.uk/MCM) has been updated by Bloss et al. (2005) based on recent improved understanding of aromatic photo-oxidation. The chemistry is developed using the protocol described by Jenkin et al. (1997) and has three previous versions: MCMv1 (Derwent et al., 1998), MCMv2 (Jenkin et al., 2000), and MCMv3 (Jenkin et al., 2003; Saunders et al., 2003), in which the aromatic chemistry is developed based on previous work and updated by new data from recent research. In addition to experimental data, many reactions are estimated from structure–reactivity relationships (SAR) method.

Several common characteristics of these mechanisms can be found. (1) The inorganic mechanisms are very similar. (2) Four organic species (methane, ethene, isoprene, and formic acid) are treated explicitly. (3) Except MCM, most of the mechanisms use lumping approaches to reduce the great number of organic reactions and/or to restrict their sizes so that emissions inventories can be used. At the same time, the chemical mechanisms have some significant differences. These differences occur in the following characteristics: (1) the lumping approaches for organic species, intermediates and products; (2) assumptions for unknown or poorly studied reactions, such as aromatics chemistry; (3) condensing processes for certain organic reactions; (4) pressure and temperature dependence of rate constants, especially for organic chemistry; (5) poorly understood photolysis parameters; (6) treatment of deposition processes or heterogeneous reactions. To focus the comparison on the mechanism itself other than the differences due to the rates or heterogeneous reactions, the last three features can be eliminated by applying the same rates for all reactions including photolysis as well as the same set of dry depositions for the modeling.

3. Method

The measurements of HO_x were performed in Houston, Texas during TRAMP-2006 campaign from August to September 2006. The simulations of HO_x were conducted in a zero-dimensional box model using each mechanism described above constrained by the same model input data measured simultaneously. This work differs from previous comparisons of mechanisms in several ways: (1) it includes the latest versions of mechanisms (SAPRC-07 and MCMv3.1) and a mechanism that has never been compared before (LaRC); (2) it is based on real atmosphere conditions; (3) it focuses on comparisons of OH and HO_2; (4) it is compared to the simultaneous *in situ* observations; and (5) it is studied for varied conditions over a month-long duration.

3.1. Site description

The latest report of Environmental Protection Agency (EPA) (EPA, 2008) shows Houston, the fourth largest metropolitan area in the United States, was still one of the areas with the highest ground-level O_3 concentrations in 2006. TRAMP was aimed at understanding air pollution in the Houston area. Further information is available at http://www.tceq.state.tx.us/nav/eq/texaqsII.html. Measurements used in this modeling comparison were made at the top of the Moody Tower on the campus of University of Houston, 60 m above the ground. The Moody Tower site (29° 43′ 3.50″ N, 95° 20′ 28.50″ W) was located at the south of the downtown area of Houston. A few kilometers to the east of this site is the Port of Houston (Ship Channel), one of the busiest sea ports in United States. However the measurement site is sufficiently far away from most individual surface emission sources and thus represents urban boundary layer conditions (Lefer and Rappenglück, 2010).

3.2. Measurements

The instruments used to measure HO_x, GTHOS (the Penn State Ground Based Tropospheric Hydrogen Oxides Sensor), is described in detail in Faloona et al. (2004) and Mao et al. (2010). Only a brief description is presented here. Air is pulled through a pin hole into a low-pressure chamber in which OH is detected by laser-induced fluorescence (LIF). OH is both excited and detected with the $A^2\Sigma^+(v'=0) \rightarrow X^2\Pi^+(v''=0)$ transition near 308 nm. HO_2 is first reacted with reagent NO to form OH and is then detected with LIF. OH and HO_2 are detected simultaneously into two low-pressure detection cells.

GTHOS is calibrated by producing known amounts of OH and HO_2 by photolyzing water vapor in high-purity air. The detection limits for OH and HO_2 are about 0.01 parts per trillion by volume (pptv) and 0.1 pptv, respectively, with a 2σ confidence level and 1-min integration time. Absolute uncertainty at the 2σ confidence level was estimated to be ±32% (Faloona et al., 2004).

Meteorological parameters, photolysis rates, gas-phase species were also measured simultaneously. Individual measurements were described in Lefer and Rappenglück (2010), Lefer et al. (in this issue), Leuchner and Rappenglück (2010), Luke et al. (2010) and Stutz et al. (2010). A brief summary of the measurements of model constraints is listed in Table 3. The good agreement between measured and calculated OH reactivity during TRAMP campaign (Mao et al., 2010) indicates that important OH reactants were all measured and included in the models.

3.3. The zero-dimensional box model

Five photochemical mechanisms (RACM, CB05, LaRC, SAPRC-99, SAPRC-07, and MCMv3.1) were applied in a zero-dimensional box model to calculate the concentrations of HO_x radicals. In order to assure that the differences of gas-phase chemical mechanisms are meaningful, several factors were standardized. Rate coefficients of reactions for all mechanisms were updated by the most recent data evaluation by Jet Propulsion Laboratory (JPL) (Sander et al., 2006) if applicable. Additional to gas-phase reactions, dry deposition rates were assigned for PAN and its analogues (0.2 cm s^{-1}) from Derwent (1996), for organic nitrates (1.1 cm s^{-1}), H_2O_2 (1.1 cm s^{-1}), CH_3OOH and its analogues (0.55 cm s^{-1}), HCHO (0.33 cm s^{-1}) from Brasseur et al. (1998), for other organic aldehydes (0.11 cm s^{-1}, assumed about 1/3 of HCHO's rate, based on Zhang et al., 2002). These rates were applied over the depth of the mixing layer (assumed 300 m at night and 1300 m for daytime, similar to Emmerson et al. (2007)). Moreover, a full set of photolysis rates were constrained in each model. The photolysis frequencies of clear sky condition were converted from the Madronich Tropospheric Ultraviolet and Visible (TUV) model (http://www.acd.ucar.edu/TUV) or calculated based on the solar zenith angle (SZA) equations in Jenkin et al. (1997) and then scaled by measurement of J_{NO2}.

Concentrations of OVOCs (except HCHO) were only available for acetaldehyde, acetone/propanal mixture, and methyl vinyl ketone (MVK)/methacrolein (MACR) mixture for about 20 days. A constant ratio of MVK/MACR (1.5 by volume ratio) was assumed based on

Table 3
Model constraints measured during TRAMP-2006.

Model parameters	Instrument/Technique	Time Interval	Uncertainty	Detection Limit	Institution
Relative humidity	Campbell HMP45C	10 s	±1%	–	UH[a]
Temperature	Campbell HMP45C	10 s	±0.2 K	–	UH
Pressure	Campbell CS105	10 s	±1 mb	–	UH
J_{NO_2}	Scanning actinic flux spectroradiometer (SAFS)	1 min	±8%	–	UH
J_{O_3}	Scanning actinic flux spectroradiometer (SAFS)	1 min	±11.5%	–	UH
NO, NO_2	Chemiluminescence (TE 42C TL)/BLD	10 s	±5.7%	50 pptv	UH
O_3	UV Photometry (TE 49C)	10 s	±2.2%	1 ppbv	UH
CO	Gas Filter Correlation (TE 48C TL)	1 min	±5.5%	2 ppbv	UH
SO_2	Pulsed Fluorescence	1 min	±5.5%	0.5 ppbv	NOAA-ARL[b]
C_2–C_{11} alkanes, alkynes	*In situ* GC-FID (Perkin–Elmer)	60 min	±5.4%	5–10 pptv	UH
C_2–C_{11} alkenes, aromatics	*In situ* GC-FID (Perkin–Elmer)	60 min	±10.2%	5–20 pptv	UH
HCHO	Hantzsch reaction fluorescence	10 min	±10%	0.15 ppbv	UH
HONO, HNO_3	Mist Chamber Ion Chromatograph	10 min	±10%	5 pptv	UNH[c]
OVOCs	PTR-MS	80 s	±50%[d]	–	TAMU[e]
Monoterpenes	PTR-MS	80 s	±50%[d]	–	TAMU

[a] University of Houston.
[b] National Oceanic and Atmospheric Administration (NOAA)'s Air Resources Laboratory (ARL).
[c] University of New Hampshire.
[d] Assumed value due to the treatment of OVOCs in Section 3.3.
[e] Texas A&M University.

Stroud et al. (2001). Median diurnal variations were used to fill the data gaps so that the modeling can be conducted for the whole campaign period. In addition, OVOCs measured by DNPH (2,4-dinitrophenylhydrazine) method at a nearby monitoring site (29° 44′ 01″ N, 95° 15′ 27″ W, 9525 Clinton Dr., 12 km east of downtown Houston) of Texas Commission on Environmental Quality (TCEQ) was used to supplement and estimate the OVOC concentrations during this campaign:

(1) A good correlation between propanal and HCHO ($R = 0.85$) was found at this site based on the measurements from August to September 2006 with a linear fit of [propanal] (in pptv) = 0.034 × [HCHO] (in pptv) + 0.14. This correlation is used to estimate the concentration of propanal based on the HCHO observed at Moody Tower.
(2) The concentration of acetone was estimated based on the concentration of the acetone/propanal mixture subtracted by the propanal concentration estimated in (1).
(3) Averaged concentrations of three carbonyl species measured at this site in August and September 2006 (0.19 ppbv of butyraldehyde, 0.32 ppbv of crotonaldehyde, and 0.13 ppbv of benzaldehyde) were assumed for these higher aldehydes.

The data of meteorological parameters, inorganic model constraints (NO, NO_2, O_3 and CO, SO_2), and photolysis rates were averaged to 10 min to be constrained in the model. Constant mixing ratios were also assumed for CH_4 (1.896 ppmv) and H_2 (500 pptv). Hourly measurements of 67 NMHCs (27 alkanes, 22 alkenes, 1 alkyne, and 17 aromatics) and 6 OVOCs were linearly interpolated to 10 min intervals used for the calculations.

The models with each mechanism were run with the FACSIMILE software (UES Software Inc.) for sufficient time so that the calculated values of HO_x and other intermediates reach instantaneous steady state. The model results with a much longer than 3-day integration time show no appreciable difference (<1%) for calculated OH and HO_2, compared to 3-day integration results. The model uncertainty at 1σ confidence level was estimated for OH and HO_2 based on Monte Carlo method (as in Carslaw et al., 1999) by applying uncertainties of kinetic rate coefficients (Sander et al., 2006) and of measurements used to constrain the models (Table 3). Uncertainties under different conditions were calculated from five typical base cases (Table 4).

4. Results

4.1. Model: measurement comparisons

4.1.1. OH

OH was measured from 11 August to 27 September 2006. Average daytime (06:00–18:00 CST) and nighttime (18:00–06:00 CST) mixing ratios were 0.33 ± 0.23 pptv (7.9×10^6 cm^{-3}) and 0.087 ± 0.066 pptv (2.1×10^6 cm^{-3}), respectively. For most days, the measured OH is generally greater than the modeled OH for all mechanisms, especially during the afternoon (e.g., on 2 Sep, Fig. 1), although there are several days the behavior of daytime OH is well captured by some models, e.g., $[OH]_{mod} = [OH]_{obs} \times 0.98$ ($R^2 = 0.82$) is found by the LaRC model on 26 Sep (Fig. 1). The diurnal cycles of the simulations for each mechanism (Fig. 2a) behave similarly. For daytime, RACM, CB05 and LaRC models have very similar diurnal cycles with higher calculated OH. SAPRC-99 and SAPRC-07 models behave similarly with lower OH. SAPRC-07 model produces about 20% more daytime OH than SAPRC-99 model. The model result of MCMv3.1 falls in the middle and is similar to RACM, CB05 and LaRC in the morning and to SAPRC-99 in the afternoon. The largest discrepancy between model and measurement occurs starting about noon and lasts the whole afternoon (11:30–17:30 CST). For all mechanisms, modeled OH is significantly less than measured OH with the average modeled-to-observed ratios of 0.69 (CB05 and RACM), 0.67 (LaRC), 0.65 (SAPRC-07), 0.59 (MCMv3.1), and 0.53 (SAPRC-99). Modeled OH only correlated with the measurement at morning rush hour ($R^2 = 0.48$–0.62 when linear fits were constrained to the origin of the coordinates) and during late afternoon ($R^2 = 0.54$–0.66). The slopes of the

Table 4
Model uncertainties calculated based on Monte Carlo method under several typical conditions.

#	CST	NO (ppbv)	NO_2 (ppbv)	O_3 (ppbv)	J_{NO_2} ($\times 10^{-3}$ s^{-1})	Modeled-to-observed ratio		Uncertainty (1σ)	
						OH	HO_2	OH	HO_2
1	8:10	7.1	12.6	30	4.3	1.86	0.73	±48%	±58%
2	12:20	0.93	4.3	87	7.7	0.66	0.67	±30%	±24%
3	16:00	0.57	2.7	78	4.0	0.62	0.65	±23%	±22%
4	23:30	3.3	18.4	11	0	0.44	0.23	±61%	±81%
5	23:30	0.14	2.4	59	0	0.26	0.44	±51%	±55%

linear regression vary from 0.81 (SAPRC-99) to 1.34 (RACM) for morning rush hour but drop to the range of 0.51 (SAPRC-99) to 0.69 (CB05) in late afternoon. Nighttime OH simulations show poor correlation with observations (R^2s are <0.19) and very low average modeled-to-observed ratios of 0.26 (SAPRC-07), 0.22 (RACM), 0.18 (CB05), 0.15 (SAPRC-99), 0.11 (MCMv3.1), and 0.06 (LaRC). This result is similar to that of other field studies that used GTHOS for OH measurements. Statistically, significant difference was observed between measured and modeled OH by all mechanisms through *t*-test at 1σ confidence level even considering the model uncertainties (Table 4) and measurement uncertainties.

4.1.2. HO_2

HO_2 was measured from 13 August to 27 September 2006. Average daytime and nighttime concentrations were 22 ± 18 pptv and 11 ± 7.8 pptv, respectively. The HO_2 calculations by each mechanism also show similar daily variation (e.g., on 29 Aug and 2 Sep, Fig. 1) but with generally lower HO_2 values. For all mechanisms, the modeled HO_2 was less than the measured HO_2, especially during the afternoon. The median diurnal cycle of HO_2 (Fig. 2b) shows the diurnal peak of 48 pptv at 13:30 CST, 1 h later than the OH peak time. This behavior is consistent with previous measurements during MCMA (Shirley et al., 2006). The modeled HO_2 (Fig. 2b) also shows similar behavior but with lower predicted concentrations for all mechanisms. Better than the correlations of OH, the correlation of observed and predicted HO_2 was good for daytime ($R^2 > 0.69$). Good agreement was found in the morning for the models with most mechanisms, except for SAPRC-99 (slope = 0.67), but especially for CB05 (slope = 0.86). The underestimates were also significant during the afternoon with lower model-to-measured ratios of 0.71 (SAPRC-07), 0.68 (CB05), 0.62 (MCMv3.1), 0.61 (LaRC), 0.60 (RACM), and 0.54 (SAPRC-99). The models with the mechanisms that produce lower OH tend to produce lower HO_2 except that the HO_2 production of SAPRC-07 model is greatly enhanced although its OH production remains relatively low. At night, the model with most mechanisms produces only 60–70% of the measured HO_2, although LaRC model is only 20% of the measured value. Similar to the comparison between measured and modeled OH, the *t*-test at 1σ confidence level indicates that the difference between measured and modeled HO_2 by all mechanisms are statistically significant.

4.1.3. HO_2/OH ratio

The ratio of HO_2 to OH has been examined in previous studies (e.g., Stevens et al., 1997; Ren et al., 2003a; Emmerson et al., 2005; Shirley et al., 2006) and used as an indicator of the cycling of OH and HO_2. During the TRAMP-2006 Campaign, the typical ratio was 30–80 with median value of 66. This ratio was observed to decrease with increasing NO concentration (Fig. 3) as expected due to the OH production from the reaction of NO with HO_2. However, all models with different mechanisms calculate a much steeper slope of HO_2/OH ratio vs. NO than is measured (Fig. 3). This difference is consistent with other field studies, including SOS (Martinez et al., 2003), PMTACS-NY2001 (Ren et al., 2003b), and PUMA (Emmerson et al., 2005). Good agreement between the modeled and measured ratios occurs when NO was about 1 ppbv. The difference among mechanisms is not obvious because modeled OH and HO_2 are both less than measured OH and HO_2. One exception is SAPRC-07 model, which yields a higher ratio because modeled HO_2 is greater than the measured HO_2 and the modeled OH is less than the measured OH.

4.2. HO_x budget

To identify the mechanism differences in simulating the production and loss processes, the average contributions of major reactions for initiation, propagation, and termination of OH and HO_2 radicals are calculated for three time periods: morning rush hour (06:00–09:00 CST), daytime (09:00–18:00 CST), and nighttime (18:00–06:00 CST) (Fig. 4).

For the modeled OH budget, RACM and CB05 models tend to yield higher OH production while SAPRC-99 model tends to yield lower production, basically consistent with the OH modeled by the

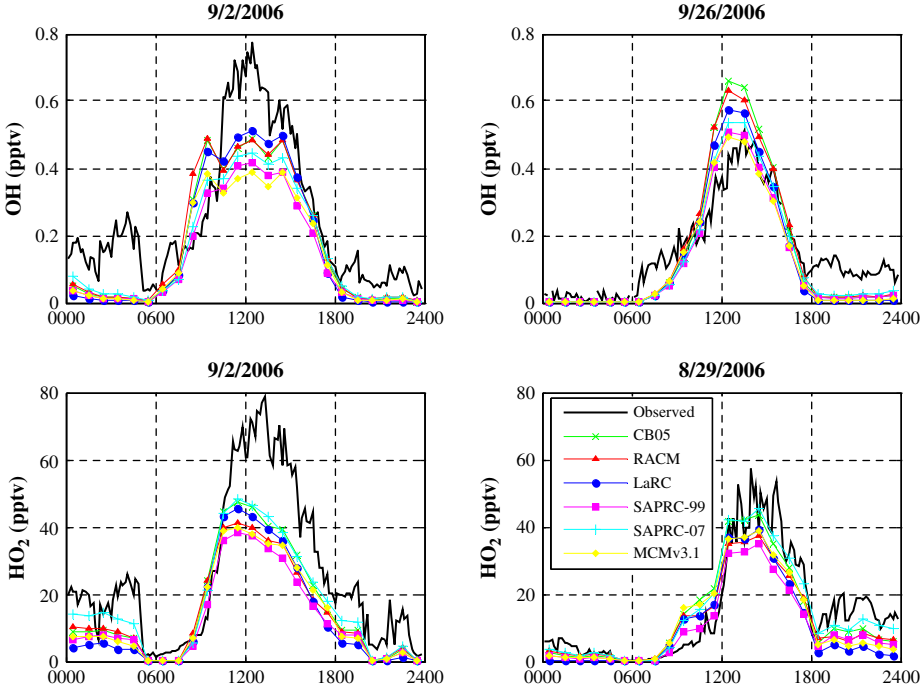

Fig. 1. Model-measurement comparison for OH (2 and 26 September) and HO_2 (29 August and 2 September). The OH mixing ratio of 0.6 pptv is equivalent to an OH concentration of about 1.4×10^7 cm^{-3}.

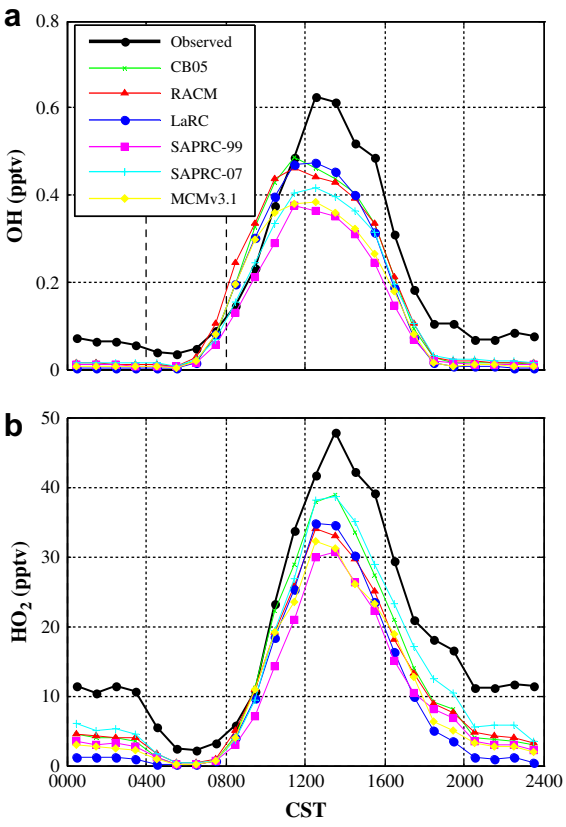

Fig. 2. Median diurnal variation of observed and modeled (a) OH and (b) HO_2 concentrations. The median values for every 1 h are shown by markers. The OH mixing ratio of 0.6 pptv is equivalent to an OH concentration of about 1.4×10^7 cm^{-3}.

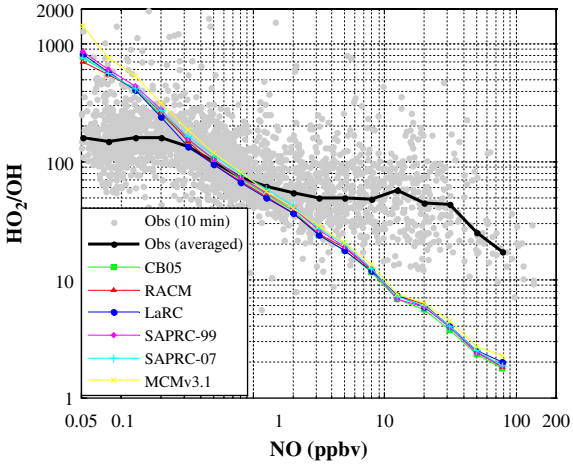

Fig. 3. Measured and modeled HO_2/OH ratio as a function of NO concentration. Grey dots are all measured HO_2/OH based on 10-min average data.

two mechanisms. The transfer from HO_2 to OH, dominated by the reaction of HO_2 with NO (>99%), comprises of more than ~85% of the OH production. The photolysis of HONO plays a very important role in OH initiation, especially in the early morning, contributing ~10% to OH formation. For the rest of the daytime, with the increase of $J(O(^1D))$, the photolysis of O_3 can compete with HONO photolysis with similar contribution of 5% for each. Only during the nighttime do the reactions of ozone with alkenes become a significant contributor (~10%) with the reaction of HO_2 with NO still dominant. The OH loss is dominated by the reactions with VOCs (~70%) and NO_x (17% during morning rush hour and 8% during other time periods), with the additional contributions from the reactions with CO and organic nitrogen. The obvious discrepancy among the mechanisms is the reactions of OH with alkenes. For instance, HO_2 is produced directly from the reaction of OH with ethene in CB05, while in other mechanisms, e.g., in RACM, only RO_2 is produced and then reacts with NO to yield HO_2. As expected, the OH budget analysis confirms that the OH production and loss are balanced in the model for all mechanisms.

For the HO_2 budget, CB05 model tends to yield higher HO_2 production while SAPRC-99 model tends to yield lower, basically consistent with the HO_2 modeled by the two mechanisms. The major contributors of HO_2 production are the conversion from RO_2 by NO (~73% combined) for all mechanisms with the exception of CB05 model (only ~30%) due to the direct formation of HO_2 from the reactions of OH with alkenes, as discussed previously. The propagation between OH and HO_2 is not balanced: the transfer from HO_2 to OH is several (2–7) times higher than the reverse process. The transfer from OH to HO_2 contributes ~20% to the total production, dominated by the reactions with OVOCs for all mechanisms except that the transfer based on CB05 model contributes much more with the percentage of ~60%. During the daytime, ~6% of HO_2 production is due to the photolysis of OVOCs, mainly the photolysis of HCHO. The contributions from the ozonolysis of alkenes are of less importance during the daytime and contribute ~ 5% during the nighttime. The loss of HO_2 is dominated by the reaction with NO (>85%), especially during the morning rush hour (>99%). The radical budget for HO_2 (Fig. 4) also shows that its production and loss are in balance in the model.

4.3. Comparison of calculated ozone production

The mechanism difference may also be reflected by the calculated instantaneous O_3 production, which can be found by the equation:

$$P(O_3) = k_{NO+HO_2}[NO][HO_2] + \sum k_i[NO][RO_2]_i \quad (1)$$

(Sadanaga et al., 2005). Therefore the differences in the calculated O_3 production by the different mechanisms will be primarily due to the differences in HO_2 and RO_2 predictions.

The modeled result of CB05 and SAPRC-07 have the highest average $P(O_3)$ of 30 ± 23 and 30 ± 22 ppbv h^{-1}, respectively, while SAPRC-99 modeled the lowest $P(O_3)$ with the magnitude of 23 ± 18 ppbv h^{-1}, which is a factor of ~1.4 lower than from CB05 and SAPRC-07 models. This result is not surprising since the predicted HO_2 by those two mechanisms was also about 1.4 times higher than modeled result of SAPRC-99. The $P(O_3)$ calculated based on RACM and LaRC fall in between these two ends and show close average production rates of ~27 ppbv h^{-1}. The calculated $P(O_3)$ for different mechanisms exhibit similar diurnal behavior (Fig. 5) of having maxima in the morning around 09:30 CST, with the magnitude of 33 ppbv h^{-1} (SAPRC-99) to 45 ppbv h^{-1} (RACM), and then continuing for about 3 h before decreasing during the afternoon. The measured concentration of O_3 (Fig. 5) peaks afternoon, which occurs an hour after the calculated $P(O_3)$ has begun to drop.

4.4. Model sensitivity

The differences between the OH and HO_2 that was measured and that was modeled with the different mechanisms were examined by two tests. The first test examined differences among the model runs with the different mechanisms as a function of some environmental parameters. The second test examined the

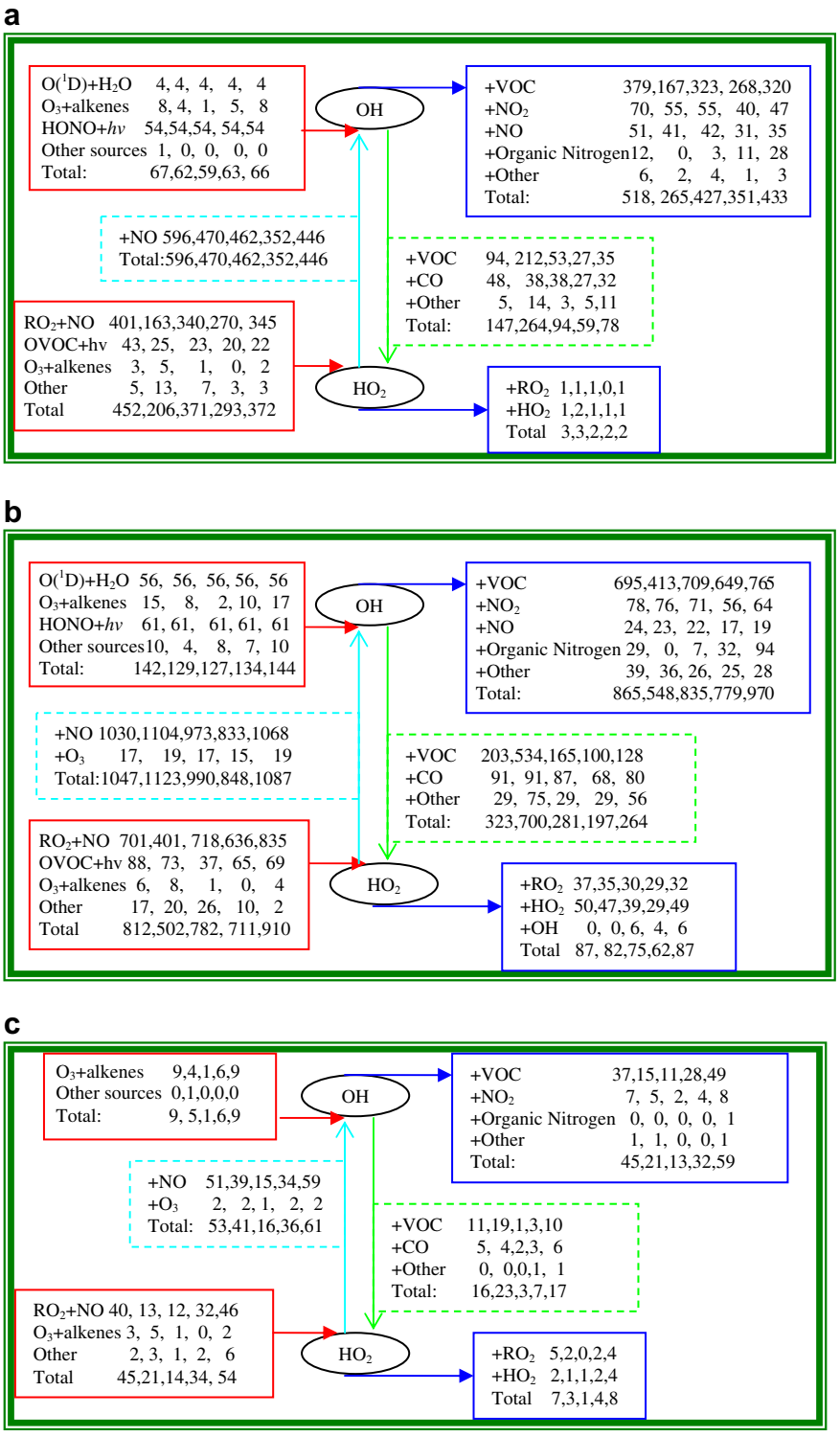

Fig. 4. Radical budget for initiation, termination, and propagation of OH and HO_2 during (a) morning rush hour (06:00–09:00 CST), (b) daytime (09:00–18:00 CST), (c) nighttime (18:00–06:00 CST), based on RACM, CB05, LaRC, SAPRC-99, and SAPRC-07. Units in 10^5 cm^{-3} s^{-1}.

possibility that an unknown HO_x source was responsible for the measured HO_x being greater than the modeled HO_x.

Differences in the model calculations of HO_x should be due to the treatment of organic chemistry. Examining the sensitivity of the model differences to environmental conditions should provide information for understanding why the different chemical mechanisms perform differently. However, the mechanism sensitivity was not easily found for any one single model constraint because some important constraints, such as NO_x, tend to correlate to others, such as VOCs.

One approach is to examine the model sensitivity to clean air versus polluted air. Daily maximum concentration of PAN

(threshold = 500 pptv) was used as an indicator to distinguish relative clean or polluted conditions. The comparison was done for the 16 days for which model-measurement comparisons were available. Conditions were classified as follows: "clean" on 27, 28 Aug, and 17, 21, 22 Sep; "polluted" on 20, 21, 29–31 Aug, and 1, 4, 6, 13, 20, 25, 26 Sep. Daily averages of ancillary measurements show that the concentrations of NO_x, O_3, CO, and NMHC were higher under polluted condition than under clean condition by a factor of about 2–3. To quantify mechanism–mechanism discrepancy, the deviation of modeling results with respect to the average of modeling results is defined here as:

$$[OH]_{dev} = ([OH]_{max} - [OH]_{min})/[OH]_{ave} \quad (2)$$

and

$$[HO_2]_{dev} = ([HO_2]_{max} - [HO_2]_{min})/[HO_2]_{ave}, \quad (3)$$

where subscript "max", "min", and "ave" represent the maximum value calculated by any mechanism for that time point, the minimum value calculated by any mechanism for that time point, and the average value of all the mechanisms for that time point, respectively. These results were then averaged over time periods and days.

The main result of this analysis was that the deviation for both modeled OH and HO_2 was larger under clean conditions than under polluted conditions. The daily average deviation was 52.8% ± 4.2% (clean) and 38.2% ± 6.1% (polluted) for OH modeling as well as 53.0% ± 2.9% (clean) and 39.2% ± 6.0% (polluted) for HO_2 modeling.

It makes sense that the model deviation should be greater in clean conditions than in polluted conditions. In polluted conditions, reactions with NO and NO_2 dominate the chemistry and control OH and HO_2 through the reaction $OH + NO_2 + M \rightarrow HNO_3 + M$, which is represented the same in all the mechanisms. Thus, the details of the organic chemistry are likely to be less important. In clean conditions, however, the reactions of HO_2 with RO_2, and RO_2 with RO_2 determine the loss rate of OH and HO_2. Thus, the amounts of

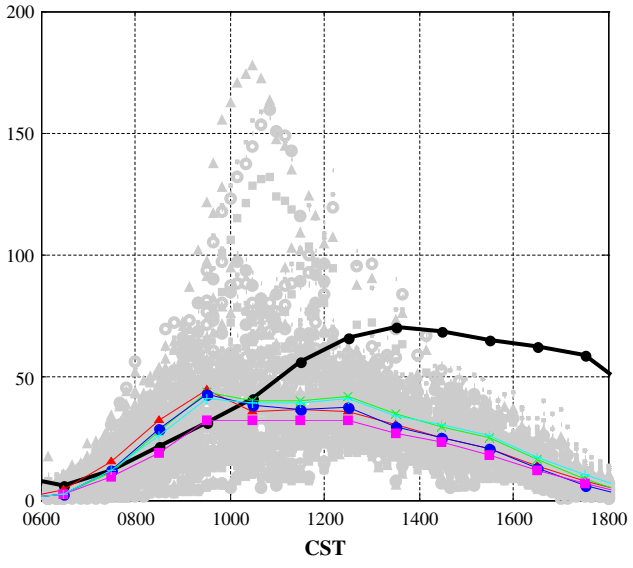

Fig. 5. Calculated ozone instantaneous production (small markers, units in ppbv h^{-1}) and its diurnal variation (lines connected markers representing the median value for each 1 h bin, units in ppbv h^{-1}) calculated by RACM (triangles), CB05 (crosses), LaRC (circles), SAPRC-99 (squares), and SAPRC-07 (pluses). The bold black line represents the diurnal variation of median concentrations of measured O_3 for each 1 h bin (black dots, units in ppbv).

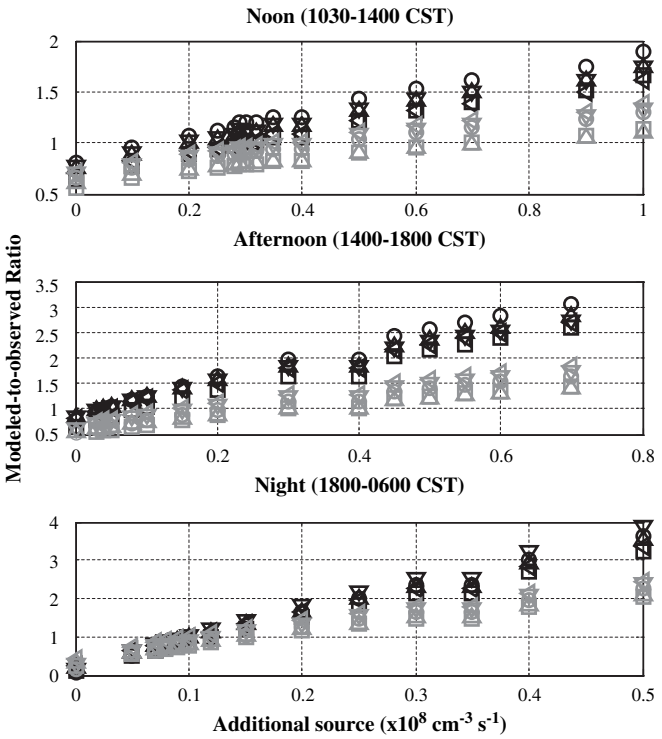

Fig. 6. The mean modeled-to-observed ratio of OH (black) and HO2 (grey) by the models with RACM (up triangles), CB05 (down triangles), LaRC (circles), SAPRC-99 (squares), SAPRC-07 (left triangles), and MCMv3.1 (diamonds) as a function of additional HO_x source (in the form of OH source) on Sep 2, 2006.

RO_2 and their reaction rate coefficients with HO_2 and each other are important in determining the OH and HO_2 amounts.

Including an additional HO_x source should improve the agreement between the modeled and measured HO_x and provide an estimate of the magnitude of possible missing sources. Because the model-measurement differences varied both day by day and during the day, the HO_x for one typical day, 2 September, was chosen for analysis, as shown in Fig. 1. The model was run with fifteen different values of an additional OH source using each mechanism. Model runs with different values of an additional OH source for all mechanisms provide an idea of the magnitude of the improvement in the model/measurement comparison for the time periods when the measured HO_x exceeded the modeled HO_x (Fig. 6). An additional OH source of 1–2 × 10^7 cm^{-3} s^{-1} brings modeled and measured HO_x into better agreement. A HO_x source of this size is equal to or greater than the known HO_x sources (please see Fig. 4). In addition, different values of additional source are required for OH and HO_2. Thus, a missing HO_x source does not resolve the model-measurement discrepancy.

5. Conclusions

Prior to this study, it was not known how OH and HO_2 calculated by a model using different mechanisms would compare to OH and HO_2 measurements in a polluted urban environment, a situation for which the chemical mechanisms were developed. The result that the modeled OH and HO_2 are generally less than the measured OH and HO_2 despite the mechanism used in the model is statistically significant. The possible reasons for this result include the following: errors in the measured precursor species or the HO_x measurements themselves; the existence of unmeasured atmospheric constituents that influence HO_x; or errors in the model or in

the chemistry that is common to all mechanisms. At present, it is not possible for us to distinguish among these possibilities. These discrepancies between measured and modeled HO_x are evident in the diurnal profiles, but cannot be resolved by the addition of an unknown HO_x source to the model.

The discrepancy between the measured and modeled behavior of the HO_2/OH ratio as a function of NO is independent of the different mechanisms. The observation of this effect by several different research groups using different measurement techniques suggests it is not an artifact of a measurement technique but is instead unknown chemistry. Because the HO_2 behavior at high NO has direct implications for the calculated ozone production rates, this issue needs to be resolved.

At the same time, the model runs with different mechanisms produce a range of HO_x values, some of which agree better with the measurements than the others, indicating that the differences are systematic and not random due to noise in the measurements of chemical species used to constrain the models. Thus, the differences between HO_x produced by the models with different mechanisms are likely the result of differences in the mechanisms themselves. It is not possible to state that any mechanism is better than another, but only that one agrees better with the measured HO_x than another during the conditions of the TRAMP-2006 study. The OH from the different model mechanisms follows the approximate order of CB05 $\gtrsim$ RACM $\gtrsim$ LaRC $\gtrsim$ SAPRC-07 $>$ MCMv3.1 $\gtrsim$ SAPRC-99 and the HO_2 follows the order SAPRC-07 $\gtrsim$ CB05 $>$ RACM $\sim$ MCMv3.1 $\gtrsim$ LaRC $>$ SAPRC-99.

This comparison of OH and HO_2 calculated by a model with several different mechanisms and measured directly applies only to the Houston site in summer 2006 and cannot a priori be applied to other environments. However, fairly complete data sets exist from numerous previous studies and even more field studies are being conducted or planned. By applying this same approach to all of these other studies, it may be possible to find patterns that will lead to a resolution of the HO_x discrepancies among the model with different mechanisms and the measurements.

Acknowledgements

We thank other participants (especially Dr. Renyi Zhang, Dr. Winston T. Luke, and Dr. Jack E. Dibb) in the TRAMP-2006 field campaign for sharing the data to make the model calculations possible. DNPH data obtained at Clinton site was made available by courtesy of Texas Commission on Environmental Quality (TCEQ). This study was supported by NSF (0209972) and HARC (TERC Project H78 and H86).

References

Bloss, C., Wagner, V., Jenkin, M.E., Volkamer, R., Bloss, W.J., Lee, J.D., Heard, D.E., Wirtz, K., Martin-Reviejo, M., Rea, G., Wenger, J.C., Pilling, M.J., 2005. Development of a detailed chemical mechanism (MCMv3.1) for the atmospheric oxidation of aromatic hydrocarbons. Atmospheric Chemistry and Physics 5, 641–664.

Brasseur, G.P., Hauglustaine, D.A., Walters, S., Rasch, P.J., Müller, J.-F., Granier, C., Tie, X.X., 1998. MOZART, a global chemical transport model for ozone and related chemical tracers 1. Model description. Journal of Geophysical Research 103, 28,265–28,289.

Carslaw, N., Jacobs, P.J., Pilling, M.J., 1999. Modeling OH, HO_2, and RO_2 radicals in the marine boundary layer 2. Mechanism reduction and uncertainty analysis. Journal of Geophysical Research 104, 30,257–30,273.

Carter, W.P.L., 1990. A detailed mechanism for the gas-phase atmospheric reactions of organic compounds. Atmospheric Environment: Part A – General Topics 24, 481–518.

Carter, W.P.L., Atkinson, R., 1996. Development and evaluation of a detailed mechanism for the atmospheric reactions of isoprene and NO_x. International Journal of Chemical Kinetics 28, 497–530.

Carter, W.P.L., May 8, 2000. Documentation of the SAPRC-99 Chemical Mechanism for VOC Reactivity Assessment. Final Report to California Air Resources Board. <http://pah.cert.ucr.edu/ftp/pub/carter/pubs/s99txt.pdf>.

Carter, W.P.L., December 31, 2007. Development of the SAPRC-07 Chemical Mechanism and Updated Ozone Reactivity Scales. Final Report to the California Air Resources Board Contract No. 03-318. <http://pah.cert.ucr.edu/~carter/SAPRC/saprc07.pdf>.

Davis, D.D., Chen, G., Chameides, W., Bradshaw, J., Sandholm, S., Rodgers, M., Schendal, J., Madronich, S., Sachse, G., Gregory, G., Anderson, B., Barrick, J., Shipham, M., Collins, J., Wade, L., Blake, D., 1993. A photostationary state analysis of the NO_2–NO system based on airborne observations from the subtropical/tropical North and South Atlantic. Journal of Geophysical Research 98, 23,501–23,523.

Derwent, R.G., 1990. Evaluation of a number of chemical mechanisms for their application in models describing the formation of photochemical ozone in Europe. Atmospheric Environment: Part A – General Topics 24, 2615–2624.

Derwent, R.G., 1993. Evaluation of the chemical mechanism employed in the EMEP photochemical oxidant model. Atmospheric Environment: Part A – General Topics 27, 277–279.

Derwent, R.G., 1996. The influence of human activities on the distribution of hydroxyl radicals in the troposphere. Philosophical Transactions of the Royal Society A: Mathematical, Physical and Engineering Sciences 354, 501–531.

Derwent, R.G., Jenkin, M.E., Saunders, S.M., Pilling, M.J., 1998. Photochemical ozone creation potentials for organic compounds in northwest Europe calculated with a master chemical mechanism. Atmospheric Environment 32, 2429–2441.

Dodge, M.C., 2000. Chemical oxidant mechanisms for air quality modeling: critical review. Atmospheric Environment 34, 2103–2130.

Emmerson, K., Carslaw, N., Carpenter, L., Heard, D., Lee, J., Pilling, M., 2005. Urban atmospheric chemistry during the PUMA campaign 1: comparison of modelled OH and HO_2 concentrations with measurements. Journal of Atmospheric Chemistry 52, 143–164.

Emmerson, K.M., Carslaw, N., Carslaw, D.C., Lee, J.D., McFiggans, G., Bloss, W.J., Gravestock, T., Heard, D.E., Hopkins, J., Ingham, T., Pilling, M.J., Smith, S.C., Jacob, M., Monks, P.S., 2007. Free radical modelling studies during the UK TORCH Campaign in Summer 2003. Atmospheric Chemistry and Physics 7, 167–181.

EPA, 2008. Latest Findings on National Air Quality – Status and Trends Through 2006. EPA-454/R-07-007. U.S. Environmental Protection Agency, Research Triangle Park, NC.

Faloona, I.C., Tan, D., Lesher, R.L., Hazen, N.L., Frame, C.L., Simpas, J.B., Harder, H., Martinez, M., Di Carlo, P., Ren, X., Brune, W.H., 2004. A laser-induced fluorescence instrument for detecting tropospheric OH and HO_2: characteristics and calibration. Journal of Atmospheric Chemistry 47, 139–167.

George, L.A., Hard, T.M., O'Brien, R.J., 1999. Measurement of free radicals OH and HO_2 in Los Angeles smog. Journal of Geophysical Research 104, 11,643–11,655.

Gery, M.W., Whitten, G.Z., Killus, J.P., Dodge, M.C., 1989. A photochemical kinetics mechanism for urban and regional scale computer modeling. Journal of Geophysical Research 94, 12,925–12,956.

Heard, D.E., Pilling, M.J., 2003. Measurement of OH and HO_2 in the troposphere. Chemical Reviews 103, 5163–5198.

Jenkin, M.E., Saunders, S.M., Pilling, M.J., 1997. The tropospheric degradation of volatile organic compounds: a protocol for mechanism development. Atmospheric Environment 31, 81–104.

Jenkin, M.E., Saunders, S.M., Derwent, R.G., 2000. Photochemical ozone creation potentials for aromatic hydrocarbons: sensitivity to variations in kinetic and mechanistic parameters. Valencia, Spain, February 27–29, 2000, ISSN 1436-2198, pp. 81–87.

Jenkin, M.E., Saunders, S.M., Wagner, V., Pilling, M.J., 2003. Protocol for the development of the Master Chemical Mechanism, MCM v3 (Part B): tropospheric degradation of aromatic volatile organic compounds. Atmospheric Chemistry and Physics 3, 181–193.

Jimenez, P., Baldasano, J.M., Dabdub, D., 2003. Comparison of photochemical mechanisms for air quality modeling. Atmospheric Environment 37, 4179–4194.

Kanaya, Y., Cao, R., Akimoto, H., Fukuda, M., Komazaki, Y., Yokouchi, Y., Koike, M., Tanimoto, H., Takegawa, N., Kondo, Y., 2007. Urban photochemistry in central Tokyo: 1. Observed and modeled OH and HO_2 radical concentrations during the winter and summer of 2004. Journal of Geophysical Research 112. doi:10.1029/2007JD008670 D21312.

Kuhn, M., Builtjes, P.J.H., Poppe, D., Simpson, D., Stockwell, W.R., Andersson-Skold, Y., Baart, A., Das, M., Fiedler, F., Hov, O., Kirchner, F., Makar, P.A., Milford, J.B., Roemer, M.G.M., Ruhnke, R., Strand, A., Vogel, B., Vogel, H., 1998. Intercomparison of the gas-phase chemistry in several chemistry and transport models. Atmospheric Environment 32, 693–709.

Lefer, B., Rappenglück, B., Flynn, J., Haman, C., 2010. Photochemical and meteorological relationships during the Texas-II Radical and Aerosol Measurement Project (TRAMP). Atmospheric Environment 44, 4005–4013.

Lefer, B., Rappenglück, B., 2010. TexAQS II Radical Measurement Project (TRAMP) overview. Atmospheric Environment 44, 4056–4067.

Leuchner, M., Rappenglück, B. VOC source–receptor relationships in Houston 1 during TexAQS-II. Atmospheric Environment, in this issue. doi:10.1016/j.atmosenv.2009.02.029.

Logan, J.A., Prather, M.J., Wofsy, S.C., McElroy, M.B., 1981. Tropospheric chemistry: a global perspective. Journal of Geophysical Research 86, 7210–7254.

Luecken, D.J., Phillips, S., Sarwar, G., Jang, C., 2007. Effects of using the CB05 vs. SAPRC99 vs. CB4 chemical mechanism on model predictions: ozone and gas-phase photochemical precursor concentrations. Atmospheric Environment. doi:10.1016/j.atmosenv.2007.08.056.

Luke, W.T., Kelley, P., Lefer, B.L., Flynn, J., Rappenglück, B., Leuchner, M., Dibb, J.E., Ziemba, L.D., Anderson, C.H., Buhr, M., 2010. Measurements of primary trace gases and NOY composition in Houston, Texas. Atmospheric Environment 44, 4068–4080.

Lurmann, F.W., Carter, W.P.L., Coyner, L.A., 1987. A Surrogate Species Chemical Reaction Mechanism for Urban-scale Air Quality Simulation Models. U.S. Environmental Protection Agency, Atmospheric Sciences Research Laboratory, Research Triangle Park, NC.

Mao, J., Ren, X., Chen, S., Brune, W.H., Chen, Z., Martinez, M., Harder, H., Lefer, B., Rappenglück, B., Flynn, J., Leuchner, M., 2010. Atmospheric oxidation capacity in the summer of Houston 2006: comparison with summer measurement in other metropolitan studies. Atmospheric Environment 44, 4107–4115.

Martinez, M., Harder, H., Kovacs, T.A., Simpas, J.B., Bassis, J., Lesher, R., Brune, W.H., Frost, G.J., Williams, E.J., Stroud, C.A., Jobson, B.T., Roberts, J.M., Hall, S.R., Shetter, R.E., Wert, B., Fried, A., Alicke, B., Stutz, J., Young, V.L., White, A.B., Zamora, R.J., 2006. OH and HO_2 concentrations, sources, and loss rates during the Southern Oxidants Study in Nashville, Tennessee, summer 1999. Journal of Geophysical Research 108, 4617. doi:10.1029/2003JD003551.

Olson, J., Prather, M., Berntsen, T., Carmichael, G., Chatfield, R., Connell, P., Derwent, R., Horowitz, L., Jin, S., Kanakidou, M., Kasibhatla, P., Kotamarthi, R., Kuhn, M., Law, K., Penner, J., Perliski, L., Sillman, S., Stordal, F., Thompson, A., Wild, O., 1997. Results from the Intergovernmental Panel on Climatic Change photochemical model intercomparison (PhotoComp). Journal of Geophysical Research 102, 5979–5991.

Ren, X., Harder, H., Martinez, M., Lesher, R.L., Oliger, A., Shirley, T., Adams, J., Simpas, J.B., Brune, W.H., 2003a. HO_x concentrations and OH reactivity observations in New York City during PMTACS-NY2001. Atmospheric Environment 37, 3627–3637.

Ren, X., Harder, H., Martinez, M., Lesher, R.L., Oliger, A., Simpas, J.B., Brune, W.H., Schwab, J.J., Demerjian, K.L., He, Y., Zhou, X., Gao, H., 2003b. OH and HO_2 chemistry in the urban atmosphere of New York City. Atmospheric Environment 37, 3639–3651.

Ren, X., Brune, W.H., Mao, J., Mitchell, M.J., Lesher, R.L., Simpas, J.B., Metcalf, A.R., Schwab, J.J., Cai, C., Li, Y., Demerjian, K.L., Felton, H.D., Boynton, G., Adams, A., Perry, J., He, Y., Zhou, X., Hou, J., 2006. Behavior of OH and HO_2 in the winter atmosphere in New York City. Atmospheric Environment 40, 252–263.

Ren, X., Olson, J.R., Crawford, J.H., Brune, W.H., Mao, J., Long, R.B., Chen, Z., Chen, G., Avery, M.A., Sachse, G.W., Barrick, J.D., Diskin, G.S., Huey, L.G., Fried, A., Cohen, R.C., Heikes, B., Wennberg, P.O., Singh, H.B., Blake, D.R., Shetter, R.E., 2008. HOx chemistry during INTEX-A 2004: observation, model calculation, and comparison with previous studies. Journal of Geophysical Research 113, D05310. doi:10.1029/2007JD009166.

Sadanaga, Y., Matsumoto, J., Kajii, Y., 2003. Photochemical reactions in the urban air: recent understandings of radical chemistry. Journal of Photochemistry and Photobiology C: Photochemistry Reviews 4, 85–104.

Sadanaga, Y., Yoshino, A., Kato, S., Kajii, Y., 2005. Measurements of OH reactivity and photochemical ozone production in the urban atmosphere. Environmental Science & Technology 39, 8847–8852.

Sander, S.P., Friedl, R.R., Ravishankara, A.R., Golden, D.M., Kolb, C.E., Kurylo, M.J., Molina, M.J., Moortgat, G.K., Keller-Rudek, H., Finlayson-Pitts, B., Wine, P.H., Huie, R.E., Orkin, V.L., 2006. Chemical Kinetics and Photochemical Data for Use in Atmospheric Studies. Evaluation Number 15 JPL Publication 06-2. NASA Jet Propulsion Laboratory, Pasadena, CA.

Saunders, S.M., Jenkin, M.E., Derwent, R.G., Pilling, M.J., 2003. Protocol for the development of the Master Chemical Mechanism, MCM v3 (Part A): tropospheric degradation of non-aromatic volatile organic compounds. Atmospheric Chemistry and Physics 3, 161–180.

Shirley, T.R., Brune, W.H., Ren, X., Mao, J., Lesher, R., Cardenas, B., Volkamer, R., Molina, L.T., Molina, M.J., Lamb, B., Velasco, E., Jobson, T., Alexander, M., 2006. Atmospheric oxidation in the Mexico City Metropolitan Area (MCMA) during April 2003. Atmospheric Chemistry and Physics 6, 2753–2765.

Stevens, P.S., Mather, J.H., Brune, W.H., Eisele, F., Tanner, D., Jefferson, A., Cantrell, C., Shetter, R., Sewall, S., Fried, A., Henry, B., Williams, E., Baumann, K., Goldan, P., Kuster, W., 1997. HO_2/OH and RO_2/HO_2 ratios during the Tropospheric OH Photochemistry Experiment: measurement and theory. Journal of Geophysical Research 102, 6379–6391.

Stockwell, W.R., 1986. A homogeneous gas phase mechanism for use in a regional acid deposition model. Atmospheric Environment 20, 1615–1632.

Stockwell, W.R., Middleton, P., Chang, J.S., Tang, X., 1990. The second generation regional acid deposition model chemical mechanism for regional air quality modeling. Journal of Geophysical Research 95, 16,343–16,367.

Stockwell, W.R., Kirchner, F., Kuhn, M., Seefeld, S., 1997. A new mechanism for regional atmospheric chemistry modeling. Journal of Geophysical Research 102, 25,847–25,879.

Stroud, C.A., Roberts, J.M., Goldan, P.D., Kuster, W.C., Murphy, P.C., Williams, E.J., Hereid, D., Parrish, D., Sueper, D., Trainer, M., Fehsenfeld, F.C., Apel, E.C., Riemer, D., Wert, B., Henry, B., Fried, A., Martinez-Harder, M., Harder, H., Brune, W.H., Li, G., Xie, H., Young, V.L., 2001. Isoprene and its oxidation products, methacrolein and methylvinyl ketone, at an urban forested site during the 1999 Southern Oxidants Study. Journal of Geophysical Research 106, 8035–8046.

Stutz, J., Oh, H.-J., Whitlow, S.I., Anderson, C., Dibb, J.E., Flynn, J.H., Rappenglück, B., Lefer, B., 2010. Simultaneous DOAS Mist-Chamber IC measurements of HONO in Houston, TX. Atmospheric Environment 44, 4090–4098.

Yarwood, G., Rao, S., Yocke, M., Whitten, G.Z., December 8, 2005. Updates to the Carbon Bond Mechanism: CB05. Final Report to the US EPA, RT-0400675. <http://www.camx.com/publ/pdfs/CB05_Final_Report_120805.pdf>.

Zhang, L., Moran, M.D., Makar, P.A., Brook, J.R., Gong, S., 2002. Modelling gaseous dry deposition in AURAMS: a unified regional air-quality modelling system. Atmospheric Environment 36, 537–560.